jmr&t
Journal of Materials Research and Technology
www.jmrt.com.br

Original article

Corrosion and wear behaviour of rice husk ash—Alumina reinforced Al–Mg–Si alloy matrix hybrid composites

Kenneth Kanayo Alaneme[a,*], *Peter Apata Olubambi*[a,b]

[a] *Department of Metallurgical and Materials Engineering, Federal University of Technology, Akure, Nigeria*
[b] *Department of Chemical and Metallurgical Engineering, Tshwane University of Technology, Pretoria, South Africa*

ARTICLE INFO

Article history:
Received 6 December 2012
Accepted 1 February 2013
Available online 14 June 2013

Keywords:
Hybrid composites
Rice husk ash
Al–Mg–Si alloy
Corrosion
Stir casting
Wear

ABSTRACT

The corrosion and wear behaviour Al–Mg–Si alloy matrix hybrid composites developed with the use of rice husk ash (RHA) and alumina as reinforcements has been investigated. Alumina added with 2, 3, and 4 wt.% RHA were utilized to prepare 10 wt.% of the reinforcing phase with Al–Mg–Si alloy as matrix using double stir casting process. Open circuit corrosion potential (OCP) and potentiodynamic polarization measurements were used to study the corrosion behaviour while coefficient of friction was used to assess the wear behaviour of the composites. The corrosion and wear mechanisms were established with the aid of scanning electron microscopy. The results show that the corrosion resistance of the single reinforced Al–Mg–Si/10 wt.% Al_2O_3 composite was superior to that of the hybrid composites in 3.5% NaCl solution, and the corrosion rates increased with increase in wt.% RHA. The increase in the population of matrix/reinforcement interface with increase in wt.% RHA in the hybrid composites was identified as the likely reason for the increase in corrosion rates observed with increase in wt.% RHA. The coefficient of friction and consequently, the wear rate of the composites were observed to increase with increase in RHA wt.%. The wear mechanism of the composites was observed to transform from predominantly abrasive wear to a combination of both adhesive and abrasive wear with increase in RHA wt.%.

1. Introduction

Aluminium matrix composites (AMCs) are noted for their unique combination of mechanical, physical and chemical properties which are scarcely attainable with the use of monolithic materials [1,2]. This has made AMCs a strong competitor to steel in terms of versatility for use in a wide range of engineering applications [3]. AMCs are currently applied in the design of components for automobiles, aircrafts, marine structures and facilities, defence assemblies, sports and recreation among many others [4–6]. Other notable advantages of AMCs are the relatively low cost of processing of [in comparison to other matrices types such as Magnesium (Mg), Copper (Cu), Titanium (Ti), Zinc (Zn)]; and its amenability to production utilizing processing techniques applied for the

* *Corresponding author.*
E-mail: kalanemek@yahoo.co.uk (K. Kanayo Alaneme).

http://dx.doi.org/10.1016/j.jmrt.2013.02.005

production of conventional monolithic metallic alloys (such as casting and powder metallurgy) [7,8]. Currently, the design of high performance aluminium based composites at significantly reduced cost is receiving much attention from materials researchers [9,10]. This is discernible from the dominant use of stir casting by most researchers from developing countries; and the sustained interest in the consideration of industrial and agro wastes as reinforcements in AMCs [11,12]. Agro waste ashes obtained by the controlled burning of agro waste products such as baggasse, bamboo leaf, coconut shell, groundnut shell, and rice husk among others; have the advantages of low densities and processing cost compared with common synthetic reinforcing ceramics such as silicon carbide and alumina [13,14]. The agro waste ashes have been successfully utilized to produce Al matrix composites with property levels which can be improved with the complement of synthetic reinforcements such as silicon carbide and alumina [15].

The design concept is built on harnessing the high strength and wear capabilities of notable synthetic reinforcements such as silicon carbide and alumina with the light weight and low cost of processing of agro waste ashes. There are very few literatures which have considered the design of AMCs with the use of hybrid reinforcements of synthetic technical ceramics and agro waste ashes. The mechanical properties of some of these low cost Al matrix composites have been reported to be encouraging depending on the weight ratio between the synthetic reinforcement and the agro waste ashes selected [15,16]. The corrosion and wear properties of these Al matrix hybrid composites are yet to receive any notable attention considering available literatures. Corrosion and wear are very important scientific phenomena requiring consideration in composite materials design to ensure material reliability in applications where they come in contact with the environment and other surfaces [17–19]. The corrosion behaviour of AMCs is widely acclaimed for its inconclusiveness judging from the often contradicting findings reported by authors for the same MMC system [20,21]. Thus it is very unlikely for the corrosion behaviour of newly developed AMCs to be predicted without subjecting them to experimental studies. The wear properties of AMCs have been reported to be dependent on factors such as the nature, size, and volume percent of the reinforcing particles [22,23]. Investigations on the wear behaviour of Al matrix hybrid composites produced with the use of agro waste ashes as complementing reinforcement are quite limited in literature. This work is an effort to understand the corrosion and wear behaviour of Al matrix composites developed using rice husk ash (RHA) and alumina as reinforcement.

2. Materials and methods

2.1. Materials

The base material for the investigation is wrought Al–Mg–Si alloy as received in form of slabs. The chemical composition of the aluminium alloy was determined using a spark spectrometric analyzer and the result is presented in Table 1. A hundred percent chemically pure alumina (Al_2O_3) particles having particle size of 28 μm and rice husk obtained from Igbemo-Ekiti, Ekiti State (a rice producing community in south western Nigeria); were utilized as reinforcing particulates. Magnesium for improvement of wettability between the Al–Mg–Si alloy and the reinforcements was also procured.

Table 1 – Elemental composition of Al–Mg–Si alloy.

Element	wt.%
Si	0.4002
Fe	0.2201
Cu	0.0080
Mn	0.0109
Mg	0.3961
Cr	0.0302
Zn	0.0202
Ti	0.0125
Ni	0.0101
Sn	0.0021
Pb	0.0011
Ca	0.0015
Cd	0.0003
Li	0.0000
Na	0.0009
V	0.0027
Al	98.88

2.2. Method

2.2.1. Preparation of RHA

A simple metallic drum with perforations to allow for air circulation to aid combustion was used as burner for the preparation of the RHA. Dry rice husks were placed inside the drum while charcoal, which served as the fire source, was used to ignite the rice husk. The husk was left to burn completely and the ashes removed 24 h later. The ash was then conditioned by heat-treating the ash at a temperature of 650 °C for 180 min to reduce the carbonaceous and volatile constituents of the ash. The chemical composition of the RHA determined using X-ray fluorescence spectroscopy is presented in Table 2.

2.2.2. Composites production

Two step stir casting process performed in accordance with Alaneme [24] was utilized to produce the composites. The process started with the determination of the quantities of RHA and alumina (Al_2O_3) required to produce 10 wt.% reinforcement consisting of 0:10, 2:8, 3:7, and 4:6 RHA and alumina weight percents, respectively. The RHA and alumina particles were initially preheated at a temperature of 250 °C to remove moisture and to help improve wettability with the Al–Mg–Si alloy melt. The Al–Mg–Si alloy ingots were charged

Table 2 – Chemical composition of the rice husk ash.

Compound/element (constituent)	wt.%
Silica (SiO_2)	91.56
Carbon	4.8
Calcium oxide CaO	1.58
Magnesium oxide, MgO	0.53
Potassium oxide, K_2O	0.39
Hematite, Fe_2O_3	0.21
others	0.93

into a gas-fired crucible furnace and heated to a temperature of 750 ± 30 °C (above the liquidus temperature of the alloy) and the liquid alloy was then allowed to cool in the furnace to a semi solid state at a temperature of about 600 °C. An external temperature probe was also used to regulate the temperature of the furnace. The preheated RHA and alumina particulates along with 0.1 wt.% magnesium were added at this temperature and stirring of the slurry was performed manually for 5–10 min. The composite slurry was then superheated to 800 ± 30 °C and a second stirring performed using a mechanical stirrer. The stirring operation was performed at a speed of 400 rpm for 10 min to help improve the distribution of the particulates in the molten Al–Mg–Si alloy. The molten composite was then cast into prepared sand moulds inserted with chills.

2.2.3. *Corrosion test*

Corrosion testing was conducted using potentiodynamic polarization electrochemical methods. The experiments were carried out using a Princeton applied research Potentiostat (VersaSTAT 400) with versaSTUDIO electrochemical software. All the experiments were performed using a three-electrode corrosion cell set-up comprising the sample as the working electrode, saturated silver/silver chloride as reference electrode, and platinum as counter electrode. Working electrodes were prepared by attaching an insulated copper wire to one face of the sample using an aluminium conducting tape, and cold mounting it in resin. The surfaces of the samples were wet ground with silicon carbide papers from 220 down to 600 grade in accordance with Alaneme and Bodunrin [25] and ASTM [26] standard, washed with distilled water, degreased with acetone and dried in air. Corrosion behaviour of the samples was investigated in 3.5% NaCl solution at room temperature (25 °C). The open circuit corrosion potential (OCP) measurements were carried out in a separate cell for 30 h. Potentiodynamic polarization measurements were carried out using a scan rate of 1.6 mV/s at a potential initiated at −200 mV to +1500 mV. After each experiment, the electrolyte was replaced, while the test samples were polished, rinsed in water and washed with acetone to remove the products that might have formed on the surface which could affect the measurement. Three repeated tests were carried out for all compositions of the composites, and the reproducibility and repeatability were observed to be good as there were no significant differences between results from triplicates.

2.2.4. *Hardness and wear test*

The hardness of the composites was evaluated using an EmcoTEST DURASCAN Microhardness Tester equipped with ecos workflow ultra modern software. Prior to testing, test specimens cut out from each composite composition were polished to obtain a flat and smooth surface finish. A load of 100 g was applied on the specimens and the hardness profile was evaluated following standard procedures. Multiple hardness tests were performed on each sample and the average value taken as a measure of the hardness of the specimen.

The wear behaviour of the single reinforced and different hybrid reinforced aluminium composites were tested using a CETR UMT-2 Tribometer. A load of 25 N was used for 1000 s, at a speed of 5 Hz.

2.2.5. *Scanning electron microscopy (SEM)*

The surface morphology of the hybrid composite samples immersed in 3.5% NaCl solution were compared with that of the single reinforced Al–Mg–Si/10 wt.% Al_2O_3 composites by recording the SEM images of the surfaces after the immersion test using a JSM 7600F Jeol ultra-high resolution field emission gun scanning electron microscope (FEG-SEM).

3. Results and discussion

3.1. *Corrosion behaviour*

Fig. 1 compares the effect of rice husk addition on the OCP stabilization curves for the single reinforced and hybrid composites produced in the 3.5% NaCl solution. The composites generally displayed a fluctuating OCP values. This was very obvious with Samples B (Al–Mg–Si/2 wt.% RHA–8 wt.% Al_2O_3 hybrid composite) and D (Al–Mg–Si/4 wt.% RHA–6 wt.% Al_2O_3 hybrid composite) and less for Sample A (single reinforced Al–Mg–Si/10 wt.% Al_2O_3 composite). This fluctuating behaviour can possibly be attributed to simultaneous corrosion products formation and breakdown. Sample A displayed relative stability of OCP followed by Sample C (Al–Mg–Si/3 wt.% RHA–7 wt.% Al_2O_3 hybrid composite). Within the period of measurement, it is observed that Sample D displayed generally the highest OCP value indicating its possibility of thermodynamic stability as compared with the other composites. Sample C had the lowest OCP value indicating that it has the highest thermodynamic tendency to corrode in the medium studied (3.5% NaCl solution).

The results for the corrosion potentials and corrosion current densities that were obtained from the potentiodynamic polarization tests for the composites (Fig. 2) are summarized in Table 3. The corrosion potentials follow similar trend with the potential values obtained in the OCP measurements (Fig. 1). The observed lower corrosion potential value on Sample AII than AI when compared with the values obtained from the OCP measurement can be attributed to its highly fluctuating OCP values. It can be observed from the OCP results that its OCP values were less than those of Sample AI between the 1300th and 1700th minutes of measurements. This can be an

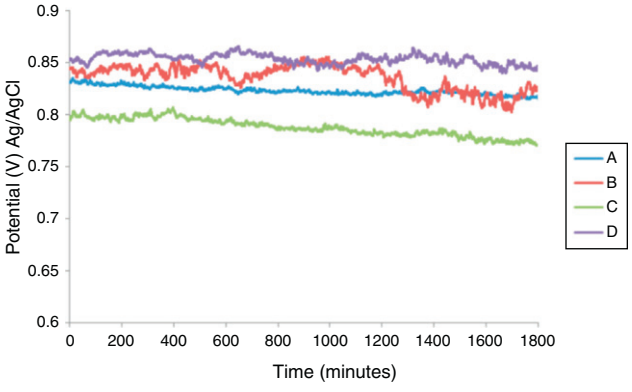

Fig. 1 – Variation of the open circuit potential with time for the single reinforced Al–Mg–Si/10 wt.% Al_2O_3 and hybrid reinforced Al–Mg–Si/RHA–Al_2O_3 composites in 3.5% NaCl solution at 25 °C.

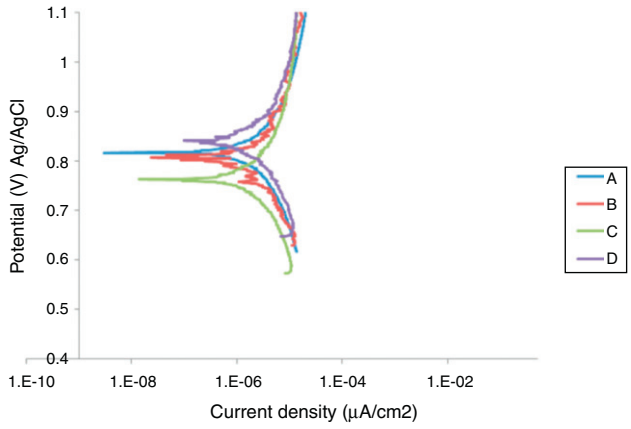

Fig. 2 – Potentiodynamic polarization curves for the single reinforced Al–Mg–Si/10 wt.% Al_2O_3 and hybrid reinforced Al–Mg–Si/RHA–Al_2O_3 composites in 3.5% NaCl solution at 25 °C.

indication that its corrosion potential will become less, indicating possible lower thermodynamic stability with time.

From Fig. 2, it is observed that the composites displayed similar polarization curves of direct passivation after the initial active corrosion where increase in corrosion current was proportional to applied potential. The corrosion current density obtained from the polarization curves, for the composites revealed relatively wide differences in the corrosion resistance. The results (Table 3) showed that the corrosion resistance of the composites decreased with increasing wt.% RHA. The single reinforced Al–Mg–Si/10 wt.% Al_2O_3 composite (Sample AI) displayed the highest corrosion resistance as revealed by its least corrosion current density value of 2.379 μA/cm^2.

Generally, corrosion of MMCs almost always initiates at a physical or chemical heterogeneity such as reinforcement/matrix interface, defect, intermetallic, mechanically damaged region, grain boundary, inclusion, or dislocation [26,27]. In alumina reinforced Al matrix composites, the corrosion mechanism has been reported to be due to the preferential initiation of corrosion in the alumina/Al matrix interface. This often occurs in form of pits or micro-crevices in the matrix near the particle–matrix interface and from regions where there is particle dropout [28]. In the case of the Al/RHA–Al_2O_3 hybrid composites, the increasing corrosion tendency with increase in wt.% RHA is likely due to the higher volume of particles arising from the low density of RHA (0.3 g/cm^3) in comparison with alumina (3.9 g/cm^3). Thus there exists a high density of particles in the hybrid composite leading to a greater number of matrix/reinforcement interfaces. The SEM images (Fig. 3a, b and d) show the surface morphology of the samples after the electrochemical test. From Fig. 3b and

Table 3 – Corrosion potentials and corrosion current densities of the produced composites.

Sample designation	Weight ratio of RHA and Al_2O_3	E_{corr} (mV)	I_{corr} (μA/cm^2)
A	0:10	816.752	2.379
B	2:8	798.422	4.209
C	3:7	763.623	6.823
D	4:6	836.234	7.614

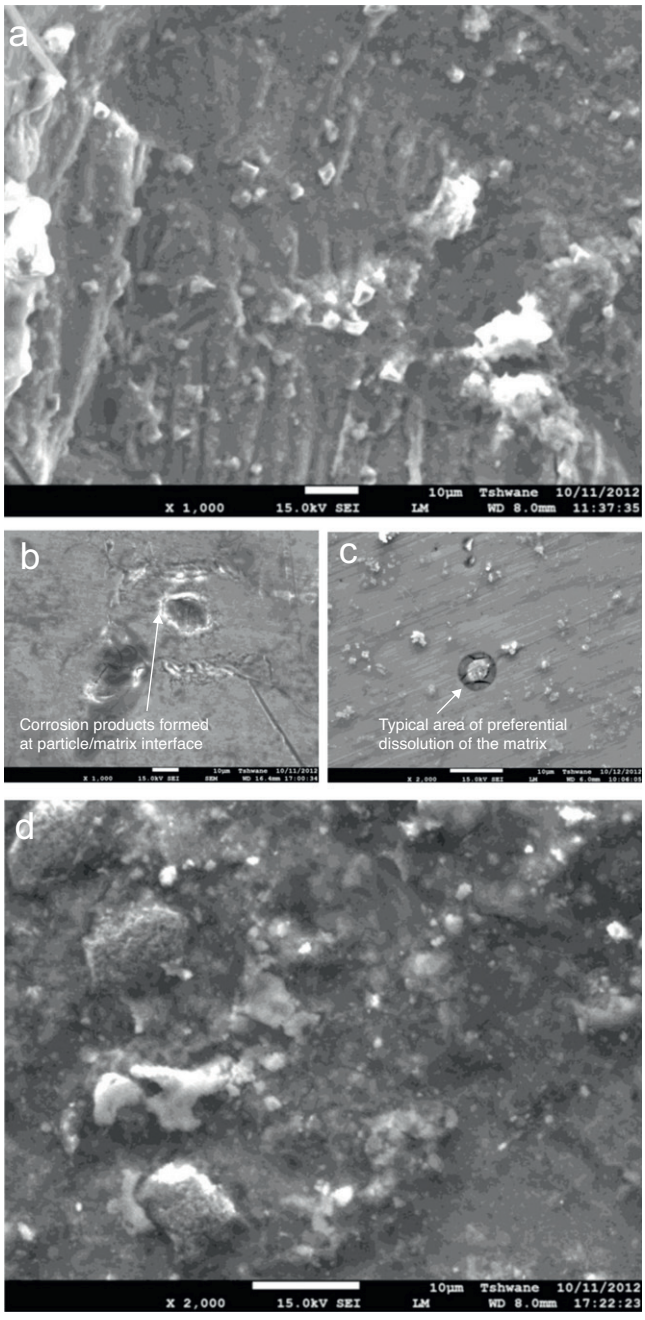

Fig. 3 – (a) SEM photomicrograph of the corroded surface of the single reinforced Al–Mg–Si/10 wt.% Al_2O_3 composite after the electrochemical test in 3.5% NaCl solution; (b) SEM photomicrograph of the corroded surface of the hybrid reinforced Al–Mg–Si/2 wt.% RHA–8 wt.% Al_2O_3 composite after the electrochemical test in 3.5% NaCl solution; (c) SEM photomicrograph of the corroded surface of the hybrid reinforced Al–Mg–Si/3 wt.% RHA–7 wt.% Al_2O_3 composite after the electrochemical test in 3.5% NaCl solution; (d) SEM photomicrograph of the corroded surface of the hybrid reinforced Al–Mg–Si/4 wt.% RHA–6 wt.% Al_2O_3 composite after the electrochemical test in 3.5% NaCl solution.

Table 4 – Composite density, percent porosity and hardness.

Sample designation	Weight ratio of RHA and Al_2O_3	Theoretical density	Experimental density	% porosity	Hardness (HVN)
A	0:10	2.82	2.791	1.028	78.6 ± 1.12
B	2:8	2.749	2.686	2.292	75 ± 0.64
C	3:7	2.713	2.661	1.917	72.2 ± 0.35
D	4:6	2.678	2.626	1.942	70 ± 0.55

c it can be confirmed that preferential dissolution of the more anodic Al matrix occurs in place of the cathodic RHA/Al_2O_3 particles.

3.2. *Hardness behaviour*

The hardness results of the composites are presented in Table 4. It is observed that the hardness decreases slightly with increase in the weight percent of RHA in the hybrid composites. The observed trend is due to the constitution of RHA which consists of over 90% of silica (SiO_2). Silica is noted to have a lower hardness level in comparison with alumina [29].

The porosity levels in the single reinforced and hybrid composites also presented in Table 4 were observed to be lower (less than 2.3%) than 4% which is the maximum porosity level acceptable in cast AMCs [5,15]. Thus its influence on the hardness properties is expected to be very marginal.

3.3. *Wear behaviour*

The variation of coefficient of friction with time is presented in Fig. 4. For all the specimens, the general observation is that there is an increase in the coefficient of friction for the first 120 s of commencing the wear test. This could be due to the hard contact surface of the counter ball used (WC ball) which results in localized adhering to the surface of the Al composites. A critical assessment of Fig. 4 shows that on the average the Al–Mg–Si/4 wt.% RHA–6 wt.% Al_2O_3 has the highest coefficient of friction in comparison to the single reinforced Al–Mg–Si matrix–10 wt.% Al_2O_3 composite and the hybrid composites containing 2 and 3 wt.% RHA. This implies that the Al–Mg–Si/4 wt.% RHA–6 wt.% Al_2O_3 hybrid composite will have a higher wear rate in comparison with

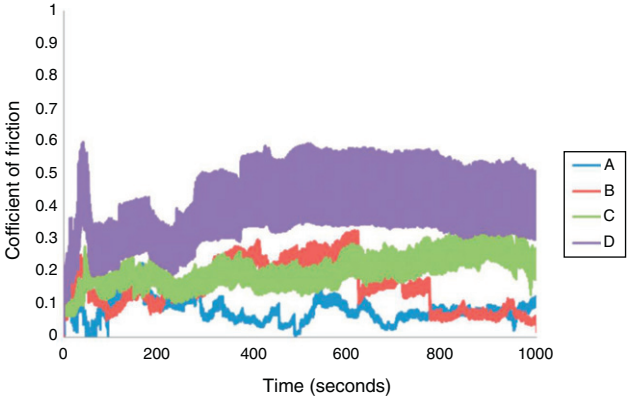

Fig. 4 – Variation of coefficient of friction with time for the single reinforced Al–Mg–Si/10 wt.% Al_2O_3 and hybrid reinforced Al–Mg–Si/RHA–Al_2O_3 composites.

the other composite compositions. Observe also that the coefficient of friction of the Al–Mg–Si/4 wt.% RHA–6 wt.% Al_2O_3 and the Al–Mg–Si/3 wt.% RHA–7 wt.% Al_2O_3 composites increases with time. This is due to an increase in the amount of debris from the composites which adheres to the surface of the Al composite resulting in increase in the friction coefficient with contact time. The single reinforced Al–Mg–Si matrix–10 wt.% Al_2O_3 composite had the least coefficient of friction an indication of its relatively lower wear rate in comparison with the hybrid composites. It is also noted that the coefficient of friction for the single reinforced Al–Mg–Si matrix–10 wt.% Al_2O_3 composite remained constant for the period of testing. The low coefficient of friction implies that the mechanism of wear is predominantly abrasive in nature due to the harder surface (tungsten carbide ball) scratching over the softer (Al–Mg–Si matrix–10 wt.% Al_2O_3 composite) surface. This argument is supported by the hardness values which shows that the single reinforced Al–Mg–Si matrix–10 wt.% Al_2O_3 composite is the hardest of the composites produced, and compared to the hybrid composites will undergo less plastic deformation and hence lower friction coefficient is to be expected [30]. Fig. 5a shows the worn tracks observed in the surface of the Al–Mg–Si matrix–10 wt.% Al_2O_3 composite. Detailed examination of the wear track of the single reinforced Al–Mg–Si matrix–10 wt.% Al_2O_3 composite reveal features associated with mainly abrasive mechanism. It is evident that the extent of adhesive wear is low compared to abrasive wear as there are few signs of worn debris attached to the surface of the sample. In the case of the 2 wt.% RHA containing hybrid composite, it is observed that the coefficient of friction increases steadily for 600 s after which there is a gradual drop in the coefficient of friction. From the variation of the coefficient of friction, it may be concluded that the initial wear mechanism for Al–Mg–Si/2 wt.% RHA–8 wt.% Al_2O_3 composite is adhesive, which converts to abrasive at a later stage. The adhesive and abrasive wear mechanisms are supported by the scanning electron micrograph of the worn Al–Mg–Si/2 wt.% RHA–8 wt.% Al_2O_3 composite (Fig. 5b). Evidence of abrasive wear is confirmed from the ploughed grooves inside the wear tracks. The signs of adhesive wear can be concluded from the patches of removed material which are glued to the worn surfaces. The patches of removed material on the surface of the composite have been reported to imply local welding at the interface and subsequent rupture of the welded joint with the formation of grooves [31,32]. For the case of the Al–Mg–Si/4 wt.% RHA–6 wt.% Al_2O_3 hybrid composite, the predominant wear mechanism is adhesive which is responsible for the increase in coefficient of friction with time. Fig. 5c shows the surface of the Al–Mg–Si/4 wt.% RHA–6 wt.% Al_2O_3 composite – observe the large accumulation of debris on the surface of the sample arising from partial welding of the debris to the surface of the composite.

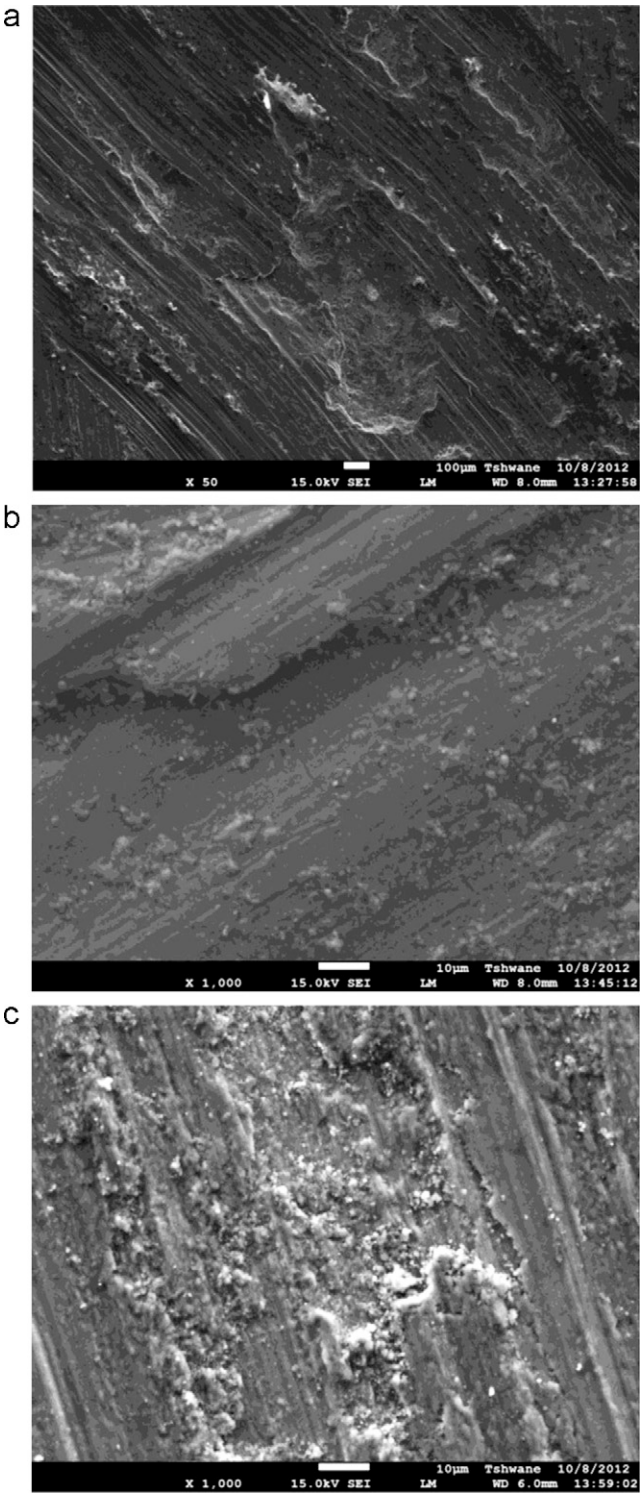

Fig. 5 – (a) SEM photomicrograph of the worn surface of the single reinforced Al–Mg–Si/10 wt.% Al_2O_3 composite; (b) SEM photomicrograph of the worn surface of the hybrid reinforced Al–Mg–Si/2 wt.% RHA–8 wt.% Al_2O_3 composite; (c) SEM photomicrograph of the worn surface of the hybrid reinforced Al–Mg–Si/4 wt.% RHA–Al_2O_3 composite.

4. Conclusions

The corrosion and wear behaviour of Al–Mg–Si matrix composites containing 0:10, 2:8, 3:7, and 4:6 wt.% RHA and alumina as reinforcement was investigated. The results show that:

- The corrosion resistance of the single reinforced Al–Mg–Si/10 wt.% Al_2O_3 composite was superior to that of the hybrid composites in 3.5% NaCl solution; and the corrosion rates increased with increase in wt.% RHA.
- The increase in the population of matrix/reinforcement interface with increase in wt.% RHA in the hybrid composites is primarily responsible for the increase in corrosion rates observed with increase in wt.% RHA.
- The coefficient of friction and consequently, the wear rate of the composites were observed to increase with increase in RHA wt.%.
- The wear mechanism of the composites was observed to transform from predominant abrasive wear to adhesive wear with increase in RHA wt.%.

Conflicts of interest

The authors declare no conflicts of interest.

REFERENCES

[1] Christy TV, Murugan N, Kumar S. A comparative study on the microstructures and mechanical properties of Al 6061 alloy and the MMC Al 6061/TiB2/12p. JMMCE 2010;9:57–65.
[2] Alaneme KK. Influence of thermo-mechanical treatment on the tensile behaviour and CNT evaluated fracture toughness of Borax premixed SiCp reinforced aluminium (6063) composites. IJMME 2012;7:96–100.
[3] Rohatgi P, Schultz B. Light weight metal matrix composites—stretching the boundaries of metals. Mater Matt 2007;2:16–9.
[4] Macke A, Schultz BF, Rohatgi P. Metal matrix composites offer the automotive industry an opportunity to reduce vehicle weight, improve performance. Adv Mater Processes 2012;170:19–23.
[5] Alaneme KK, Aluko AO. Fracture toughness (K_{1C}) and tensile properties of as-cast and age-hardened aluminium (6063)—silicon carbide particulate composites. Sci Iran Trans A 2012;19:992–6.
[6] Miracle DB. Metal matrix composites—from science to technological significance. Compos Sci Technol 2005;65:2526–40.
[7] Surappa MK. Aluminium matrix composites: challenges and opportunities. Sadhana 2003:319–34, 281 & 2.
[8] Adiamak M. Selected properties of aluminium alloy based composites reinforced with intermetallic particles. JAMME 2006;14:43–7.
[9] Zuhailawati H, Samayamutthirian P, Mohd Haizu CH. Fabrication of low cost aluminium matrix composite reinforced with silica sand. J Phys Sci 2007;18:47–55.
[10] Maleque MA, Atiqah A, Talib RJ, Zahurin H. New natural fibre reinforced aluminium composite for automotive brake pad. IJMME 2012;7:166–70.
[11] Mahendra KV, Radhakrisna A. Characterization of stir cast Al–Cu–(fly ash + SiC) hybrid metal matrix composites. J Comp Mater 2010;44:989–1005.

[12] Madakson PB, Yawas DS, Apasi A. Characterization of coconut shell ash for potential utilization in metal matrix composites for automotive applications. IJEST 2012;4:1190–8.
[13] Prasad SD, Krishna RA. Production and mechanical properties of A356. 2/RHA composites. IJSAT 2011;33:51–8.
[14] Aigbodion VS, Hassan SB, Dauda ET, Mohammed RA. Experimental study of ageing behaviour of Al–Cu–Mg/bagasse ash particulate composites. Tribology in Industry 2011;33:28–35.
[15] Alaneme KK, Akintunde IB, Olubambi PA, Adewale TM. Mechanical behaviour of rice husk ash—alumina hybrid reinforced aluminium based matrix composites. J Mater Res Technol 2013;2(1):60–7.
[16] Escalera-Lozano R, Gutierrez C, Pech-Canul MA, Pech-Canul MI. Degradation of Al/SiCp composites produced with rice–hull ash and aluminium cans. Waste Manage 2008;28:389–95.
[17] Alaneme KK. Corrosion behaviour of heat-treated Al-6063/SiC_p composites immersed in 5 wt% NaCl solution. Leonardo J Sci 2011;18:55–64.
[18] Bobic B, Mitrovic S, Bobic M, Bobic I. Corrosion of metal matrix composites with aluminium alloy substrate. Tribol Ind 2010;32:3–11.
[19] Suresha S, Sridhara BK. Friction characteristics of aluminium silicon carbide graphite hybrid composites. Mater Des 2012;34:576–83.
[20] Pinto GM, Jagannath N, Shetty AN. Corrosion behavior of 6061 Al–15 vol. pct. SiC composite and its base alloy in mixture of 1:1 hydrochloric and sulphuric acid medium. Int J Electrochem Sci 2009;4:1452–68.
[21] Dolata AJ, Dyzia M, Walke W. Influence of particles types and shape on the corrosion resistance of aluminium hybrid composites. Solid State Phenom 2012;191:81–7.
[22] Ravi Kumar K, Mohanasundaram KM, Arumaikkannu G, Subramanian R. Analysis of parameters influencing wear and frictional behaviour of aluminium–fly ash composites. Tribol Trans 2012;55:723–9.
[23] Gaitonde V, Karnik S, Jayaprakash M. Some studies on wear and corrosion properties of Al5083/Al_2O_3/graphite hybrid composites. JMMCE 2012;11:695–703.
[24] Alaneme KK. Mechanical behaviour of cold deformed and solution heat-treated alumina reinforced AA 6063 composites. West Indian J Eng 2013;35(2):31–5.
[25] Alaneme KK, Bodunrin MO. Corrosion behaviour of alumina reinforced Al (6063) metal matrix composites. JMMCE 2011;10:1153–65.
[26] ASTM, G5-94. Annual Book of ASTM Standards, Standard Reference test Method for Making Potentiostatic and Potentiodynamic Anodic Polarization, Measurements, vol. 3; 2000. p. 57–67.
[27] Mishra AK, Balasubramaniam R, Tiwari S. Corrosion inhibition of 6061-SiC by rare earth chlorides. Anti-Corros Methods Mater 2007;54:37–46.
[28] Reena Kumari PD, Nayak J, Nityananda Shetty A. Corrosion behavior of 6061/Al-15 vol. pct. SiC(p) composite and the base alloy in sodium hydroxide solution. Arabian J Chem 2011, http://dx.doi.org/10.1016/j.arabjc.2011.12.003.
[29] Courtney TW. Mechanical Behaviour of Materials. 2nd ed. India: Overseas Press; 2006.
[30] Onat A. Mechanical and dry sliding wear properties of silicon carbide particulate reinforced aluminium–copper alloy matrix composites produced by direct squeeze casting method. J Alloys Compd 2010;489:119–24.
[31] Alidokht SA, Abdollah-zadeh A, Soleymani S, Assadi H. Microstructure and tribological performance of an aluminium alloy based hybrid composite produced by friction stir processing. Mater Des 2011;32:2727–33.
[32] Łągiewka M, Konopka Z, Zyska A, Nadolski M. Examining of abrasion resistance of hybrid composites reinforced with SiC and C_{gr} particles. Arch Foundry Eng 2008;8:59–62.